

PAPER

Fish-like three-dimensional swimming with an autonomous, multi-fin, and biomimetic robot

To cite this article: F Berlinger *et al* 2021 *Bioinspir. Biomim.* **16** 026018

View the [article online](#) for updates and enhancements.



IOP | ebooks™

Bringing together innovative digital publishing with leading authors from the global scientific community.

Start exploring the collection—download the first chapter of every title for free.

Bioinspiration & Biomimetics



PAPER

Fish-like three-dimensional swimming with an autonomous, multi-fin, and biomimetic robot

RECEIVED
10 August 2020

REVISED
2 November 2020

ACCEPTED FOR PUBLICATION
2 December 2020

PUBLISHED
10 February 2021

F Berlinger^{1,*} , M Saadat² , H Haj-Hariri³, G V Lauder² and R Nagpal¹

¹ Harvard University, John A. Paulson School of Engineering and Applied Sciences, Cambridge, MA 02138, United States of America

² Department of Organismal and Evolutionary Biology, Harvard University, Cambridge, MA 02138, United States of America

³ College of Engineering and Computing, University of South Carolina, Columbia, SC 29208, United States of America

* Author to whom any correspondence should be addressed.

E-mail: fberlinger@seas.harvard.edu

Keywords: underwater robot, fish swimming, multiple fins, autonomous, maneuverable, particle image velocimetry

Supplementary material for this article is available [online](#)

Abstract

Fish migrate across considerable distances and exhibit remarkable agility to avoid predators and feed. Fish swimming performance and maneuverability remain unparalleled when compared to robotic systems, partly because previous work has focused on robots and flapping foil systems that are either big and complex, or tethered to external actuators and power sources. By contrast, we present a robot—the Finbot—that combines high degrees of autonomy, maneuverability, and biomimicry with miniature size (160 cm³). Thus, it is well-suited for controlled three-dimensional experiments on fish swimming in confined laboratory test beds. Finbot uses four independently controllable fins and sensory feedback for precise closed-loop underwater locomotion. Different caudal fins can be attached magnetically to reconfigure Finbot for swimming at top speed (122 mm s⁻¹ \equiv 1 BL s⁻¹) or minimal cost of transport (CoT = 8.2) at Strouhal numbers as low as 0.53. We conducted more than 150 experiments with 12 different caudal fins to measure three key characteristics of swimming fish: (i) linear speed-frequency relationships, (ii) U-shaped CoT, and (iii) reverse Kármán wakes (visualized with particle image velocimetry). More fish-like wakes appeared where the CoT was low. By replicating autonomous multi-fin fish-like swimming, Finbot narrows the gap between fish and fish-like robots and can address open questions in aquatic locomotion, such as optimized propulsion for new fish robots, or the hydrodynamic principles governing the energy savings in fish schools.

1. Introduction

Fish are excellent swimmers, navigating cluttered environments such as coral reefs in search of food, migrating long distances in the ocean, or swimming up rivers to reproduce. In doing so, fish combine a high degree of maneuverability with effective long-distance swimming, a combination that is highly attractive from an engineering perspective. Fish can achieve this level of performance in part by using multiple fins to vector forces in three dimensions, supported by sensory systems for closed-loop control of fin kinematics. Fish-inspired robots with high maneuverability, multi-fin control, and effective cruise capability would significantly expand the application range of autonomous and self-propelled underwater robots.

Biologists have made great strides in understanding aquatic locomotion [1, 2]. Many fish generate propulsive thrust by using body undulations to accelerate the surrounding fluid backwards [1, 3–6]. The oscillation of body and tail typically leaves behind a trail of counter-rotating vortices whose mutual interactions produce a desired backwards jet of fluid known as reverse Kármán wake [7]. When time averaged, this wake shows a central high-speed jet indicative of a thrust-producing flapping appendage. The strength of the jet correlates with swimming speed and depends on both the frequency of vortex shedding and tail beating. It is observed that the swimming speed of diverse species of fish is roughly linearly proportional to their tail beat frequency [8, 9]. Moreover, fish often exhibit a U-shaped curve for the energetics of swimming when described as cost of transport

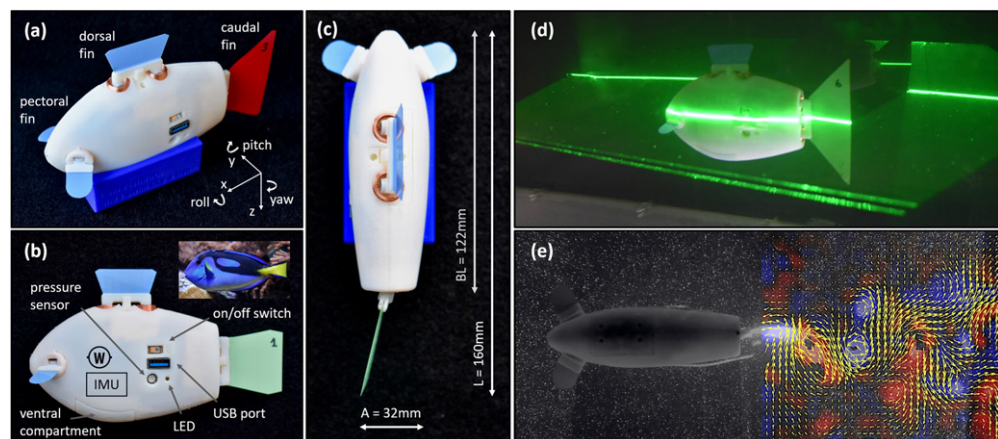


Figure 1. Finbot: an autonomous and biomimetic experimental platform. (a) Finbot was designed to enable autonomous fish-like swimming. Four independently controllable flexible fins enable precise maneuvers in 3D space (x , y , z corresponding to surge, sway, heave). The caudal fin connects magnetically to the main body and can be exchanged easily to alter swimming speed and CoT. (b) The rigid and streamlined body is inspired in shape by fish such as the blue tang (depicted top right⁴). Finbot swims autonomously in 3D, using an inertial sensor (IMU) to control heading and a pressure sensor to control depth, and can monitor its own power consumption. (c) Tail beat amplitude A was tuned to approximately 20% of the body length L (including fin) according to the observed value among a diverse species of fish [44]. (d) Finbot in a laser light imaging with particle image velocimetry, which was used to visualize wake structures. (e) A trailing wake behind Finbot; several wakes were similar to reverse Kármán streets, which are characteristic of fish swimming.

(CoT) [10–12]. CoT ($= P/mgU$), is nondimensional and defined here as the metabolic power, P , per body weight, mg , per swimming speed, U . In addition, the Strouhal number, $St (= fA/U)$, is a widely used indicator for the effectiveness of flapping motion [9, 13]. St describes the relative distance a swimmer advances per beat of its tail, with A being the tail beat amplitude, measured as the tip-to-tip excursion of the tail. Based on these biological observations, one can define the following three key criteria for robots to exhibit fish-like swimming: (i) vortices are shed from the flapping caudal fin such that a reverse Kármán wake forms; (ii) the tail beat frequency is linearly correlated with the swimming speed; and (iii) CoT is U-shaped with a minimum at intermediate swimming speeds.

Insights on aquatic locomotion have inspired roboticists to design fish-like propulsors [14–19] and robotic systems [20–41]. However, many engineered systems fall short of accurately mimicking fish swimming or achieving fish-like performance, and rely on open-loop control of single fins. One class of fish-like experimental platforms are flapping propulsors, composed of single fins or foils attached to external actuators above the waterline [14–17]. While useful as simple physical models for the study of swimming performance including metrics such as CoT [18, 19], such propulsors are neither autonomous nor freely-swimming compared to real fish. Another group of self-propelled fish-like robots are large in scale and complex [20–22], and designed to operate in open water rather than serve as experimental platforms in the laboratory. Robots which have been used for laboratory studies are often held in place by a harness or tethered [22–26, 32] because it is challenging to integrate power and sensing

autonomy in a small enough and maneuverable design. Despite restricted maneuverability, tethered robots that are free-swimming can be useful to study fish locomotion. The systems featuring soft actuation technologies are mostly underpowered, which makes production of fish-like swimming speeds difficult [27–29]. Overall, few robots are autonomous and free swimming [20, 21, 27–31, 33–38, 42], or fish-like [20, 25, 30, 31, 33–38, 42]. Often, fish-inspired robots struggle to reconcile key parameters associated with fish-like swimming: self-propulsion, the ability to control body position in three dimensions, maneuverability, and low-cost effective cruising. Accordingly, there is a gap in the current device space: autonomous, maneuverable, and biomimetic multi-fin underwater robots [supplemental table S1 (<https://stacks.iop.org/BB/16/026018/mmedia>)].

The goal of this paper was to demonstrate fish-like swimming including properties such as U-shaped costs of transport and reverse Kármán wakes with a biomimetic robot named Finbot (figure 1). To the best of our knowledge, Finbot is the first and smallest multi-fin autonomous underwater robot that also faithfully replicates multiple characteristics of fish swimming. While based on our own previous work [30], Finbot was significantly upgraded with an exchangeable caudal fin, an onboard power monitor, and a more streamlined and biomimetic body shape to enable this study.

2. Methods

2.1. The Finbot platform

Finbot enhances an earlier robot for three-dimensional (3D) multi-fin swimming presented in our previous work [30]. Both robots have four

independently controllable fins. Two pectoral fins and a caudal fin allow for turning, stopping, and forward motions in the horizontal surge-sway plane. These horizontal motions, guided by sensory feedback from an onboard inertial measurement unit (IMU), are decoupled from vertical diving along the heave axis. The robots are passively stable in roll and pitch, and slightly positively buoyant, so that they float toward the water surface unless the dorsal fin is activated for controlled diving using depth estimates from a pressure sensor.

In Finbot's design, we focused on two main goals: (i) to generate fish-like locomotion by careful selection of flexible caudal fins which can produce reverse Kármán wake structures; (ii) to achieve self-propelled and controlled motions in 3D space, whose performance metrics such as speed and CoT are reminiscent of fish. In the Results, we highlight Finbot's new features including an updated body shape inspired by the blue tang (*Paracanthurus hepatus*), upgraded electronics for higher performance and power consumption monitoring, and a modular magnetic mechanism for testing different caudal fins. Additional information on the design, components, and fabrication is in section 1 of the supplement.

2.2. Closed-loop controlled multi-fin free swimming

A high degree of maneuverability compared to most underwater robots of similar size (supplemental table S1) allows Finbot to follow a wide range of 3D trajectories as we showed previously [30]. Here, we focused on submerged straight-line swimming, for which the caudal fin operates at a constant frequency to generate thrust in surge-direction while the pectoral fins are used to correct any deviations from a straight course by effecting turning around the yaw-axis. The frequencies of the pectoral fins are adjusted continuously between 2 Hz to 8 Hz with a proportional–integral–derivative (PID) closed-loop controller to modulate the thrust force according to the momentary deviation from a straight-line trajectory (supplemental figure S2). Such deviations are detected from time-averaged IMU readings, whereby the robot and IMU, respectively, are initialized in alignment with the straight-line target direction. Using the implemented closed-loop controllers, Finbot can maintain a submerged straight-line course. However, small errors accumulate over time due to drift on the IMU of approximately $0.5^\circ/\text{min}$ in yaw. Additional information on controller design and depth control is in movie S3 and section 2 of the supplement.

2.3. Caudal fin settings for various tail beat frequencies and fin geometries

We tested a variety of caudal fins at different tail beat frequencies, and the amplitude of caudal fin oscillation was always mechanically constrained at the pivot

of the caudal peduncle. In order to achieve consistent peak-to-peak amplitudes at the tip of different fins across all frequencies, we adjusted the input power to the caudal actuator with pulse width modulation. For each fin and frequency, we took slow motion videos at five different input powers to visually select the power setting that optimally matched the fin's peak-to-peak travel time with the prescribed oscillation period. In addition, we chose a sinusoidal input signal to enhance smooth changes of direction at peak amplitude where input power is minimal, and therefore a more undulatory fin motion.

2.4. Experimental setup and measurement devices for drag and particle image velocimetry

All experiments were conducted in fresh water in a laboratory flow tank [3] that consisted of a $66\text{ cm} \times 28\text{ cm} \times 28\text{ cm}$ (l, w, h) large test section (supplemental figure S3(A)). The water remained stationary except for separate experiments tuning the PID controllers and measuring the drag of the robot body. Drag was measured on a 3D-printed robot dummy attached to a six-axis force/torque sensor (ATI Nano17) above the waterline. For each of six different flow speeds ranging from 30 mm s^{-1} to 200 mm s^{-1} , data was collected at a sampling rate of 1000 Hz for 120 s and time-averaged to a single mean and standard deviation after removing the auto-correlation in the signal.

We recorded video of experiments with a Photron Mini-UX100 high-speed camera at 250 frames/sec and a resolution of 1280×1024 pixels. For the visualization of vortices shed from the caudal fin and the corresponding wake structures, microparticles ($50\text{ }\mu\text{m}$ mean size) were added to the water and an Opto Engine 5 W argon-ion laser in conjunction with a Powell lens generated a horizontal light sheet directed at Finbot. Pairs of sequential video frames were processed with DaVis 8.4 software (LaVision Inc., Göttingen Germany) to generate a time series of velocity vector fields throughout the tail beat cycle. Finbot surrounded by microparticles and illuminated by the laser light with its trailing wake visualized is shown in figure 1(e) and movie S2.

2.5. Testing routines and data processing for swimming speed and power consumption

For all experiments, Finbot was initialized on the water surface and aligned with the target swimming direction at the right end of the 66 cm long test section for a period of 15 s during which steady-state drift and surface pressure were measured. Finbot was then carefully released at the programmed target depth of 15 cm below surface and swam toward the other left end of the test section within 5 s to 22 s, depending on its cruise speed (movie S1 and supplemental figure S3). We repeated test runs five and three times at each tail beat frequency for figures 2–4, respectively, and reported the mean and standard deviation for swimming performance metrics.

Table 1. Equation terms.

m	Body mass
mg	Body weight
L	Characteristic length
CoT	Cost of transport
C_D	Drag coefficient
ρ	Fluid density
ν	Kinematic fluid viscosity
S_d	Lateral planform area
P	Power
D	Resistive drag
Re	Reynolds number
St	Strouhal number
U	Swimming speed
A	Tail beat amplitude
f	Tail beat frequency
F	Thrust force

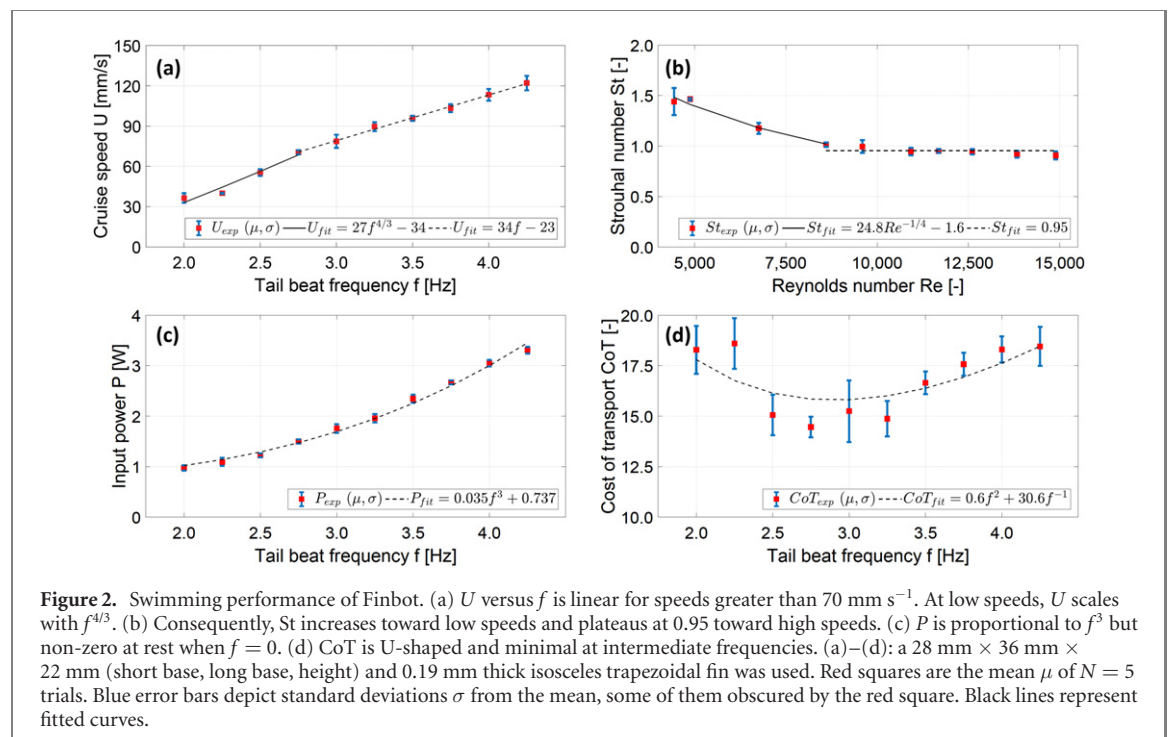


Figure 2. Swimming performance of Finbot. (a) U versus f is linear for speeds greater than 70 mm s^{-1} . At low speeds, U scales with $f^{4/3}$. (b) Consequently, St increases toward low speeds and plateaus at 0.95 toward high speeds. (c) P is proportional to f^3 but non-zero at rest when $f = 0$. (d) CoT is U-shaped and minimal at intermediate frequencies. (a)–(d): a $28 \text{ mm} \times 36 \text{ mm} \times 22 \text{ mm}$ (short base, long base, height) and 0.19 mm thick isosceles trapezoidal fin was used. Red squares are the mean μ of $N = 5$ trials. Blue error bars depict standard deviations σ from the mean, some of them obscured by the red square. Black lines represent fitted curves.

Swimming speeds at steady-state cruise, i.e. after an initial acceleration period, were deduced from recorded videos with the help of a deep convolutional neural network [43] (supplement section 3.1). Power consumption for forward propulsion was measured with an onboard power monitor at a sampling rate of approximately 30 Hz (supplement section 3.2), whereby only the input power to the caudal fin was considered. Consequently, our reported CoT must be understood as the cost of forward propulsion effected by the caudal fin, and not the total CoT utilizing all fins.

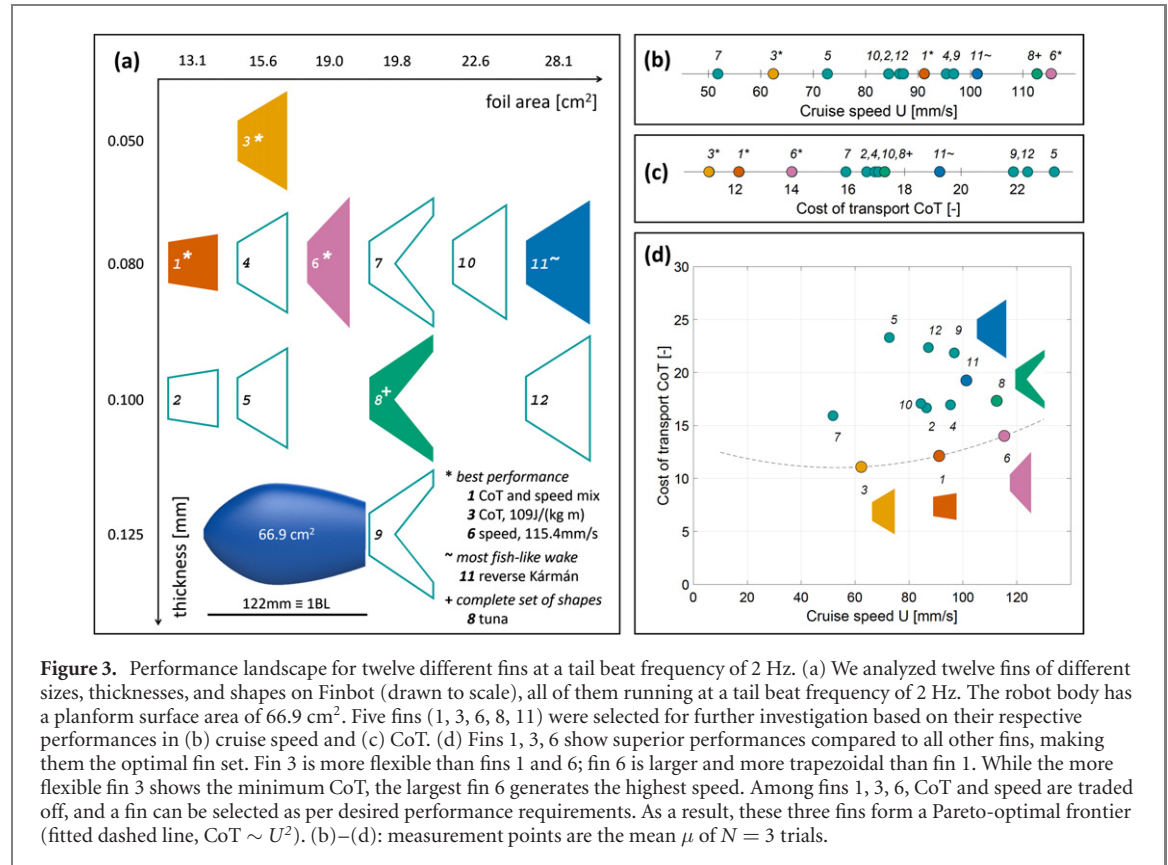
2.6. Live fish experiments with bluegill sunfish

Bluegill sunfish (*Lepomis macrochirus*) swam in a recirculating flow tank and data on steady undulatory body locomotion and wake flow patterns were obtained at speeds ranging from 0.5 BL s^{-1} to 2.5 BL s^{-1} . Wake flow patterns were visualized by

seeding the water with small ($12 \text{ }\mu\text{m}$ mean size) silver-coated glass beads, and by imaging water flow patterns in the wake of the caudal fin using a Redlake MotionScope PCI 500 high-speed camera system operating at 250 frames/sec and $1/1000 \text{ s}$ shutter speed. An 8 W argon-ion continuous wave laser (Coherent Inc., Santa Clara, CA, USA) was focused into a thin light sheet ($1\text{--}2 \text{ mm}$ thick) that illuminated the reflective particles. We used DaVis 8.4 software to perform cross-correlation analyses using standard PIV algorithms as in our previous research.

2.7. Scaling laws for speed, Strouhal number, drag coefficient, power, and cost of transport

Fish and Finbot are subject to natural scaling laws with regard to their aquatic locomotion. In cruise, thrust generated by the tail is balanced with the drag experienced by the body and so St is only a function of the shape of the robot and scales approximately



with the square root of drag coefficient for streamlined objects, $\text{St} \sim C_d^{1/2}$ [44], where $C_d = 2D/\rho U^2 S_d$ with D being the resistive drag, ρ the density of the fluid, and S_d the lateral planform area of the tail and body (table 1 defines all equation terms). For laminar flow regime at low speeds, the drag coefficient of thin streamlined objects scales approximately as $\text{Re}^{-1/2}$ [44, 45], where $\text{Re} = UL/v$ is the Reynolds number with L being the characteristic length of the swimmer, and v the kinematic viscosity of the fluid. As a result, St scales as $\text{Re}^{-1/4}$, and U with $f^{4/3}$ for constant flapping amplitudes. For high speeds associated with turbulent flow, C_d and St remain relatively constant [44, 45], and U scales linearly with f .

Input power scales as $P \sim \rho S_d (fA)^2 (fL)$ for purely pitching foils (as surrogates for the caudal fin of Finbot) based on inviscid hydrodynamics theory and supported by experimental data [46, 47]. For self-propelled underwater robots such as Finbot, a finite amount of energy is required to propel from rest since some energy is lost due to the internal mechanical and electrical inefficiencies. Thus, in practice, the input power approaches a constant greater than zero as flapping frequency approaches zero and so, $P \sim \rho S_d (fA)^2 (fL) + a$, where $a (> 0)$ is a constant.

Assuming swimming modes with constant flapping amplitude and mass, CoT then scales as:

$$\text{CoT} = \frac{P}{(mg)U} \sim \rho S_d \text{St}^3 \left(\frac{L}{A} \right) U^2 + \frac{a}{U} \quad (1)$$

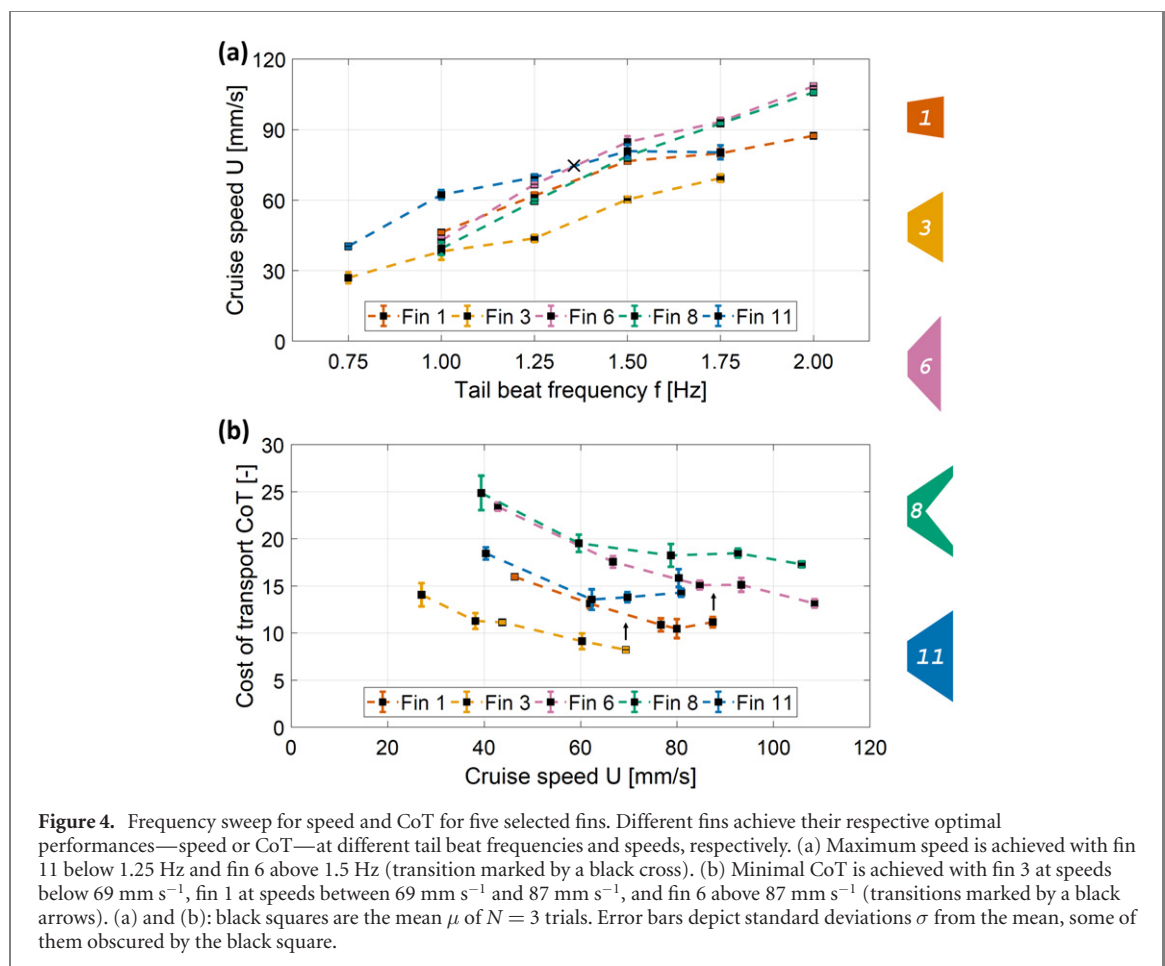
The first term in equation (1) increases with speed as $U^{5/4}$ for low speeds at which St scales as $\text{Re}^{-1/4}$, and as U^2 for high speeds where St remains relatively constant. The second term decreases in proportion with the inverse of the speed, $1/U$. The addition of the two terms as in equation (1) then results in one value for speed such that CoT is minimized.

3. Results

Finbot is the first autonomous and biomimetic multi-fin platform small enough for the laboratory investigation of 3D fish-like swimming under closed-loop control. This section highlights newly designed key aspects of the robot, followed by a range of experiments to explore the performance landscape of different caudal fins and demonstrate fish-like swimming.

3.1. The design of Finbot enables multi-fin autonomous self-propelled swimming

Finbot is self-propelled and completely autonomous, using four independently controllable fins and feedback from an IMU and pressure sensor for submerged free swimming (see Methods). Due to the four fins, Finbot is highly maneuverable and capable of following a large range of prescribed trajectories, which supports the design of various experiments. Since Finbot is also small, such experiments can be conducted in the same flow tanks used for laboratory studies on fish, where data acquisition including PIV is most straightforward, reliable, and efficient. The



design of Finbot (figure 1) was guided by observations on fish swimming, and its streamlined shape was inspired by measured body dimensions of the blue tang (*P. hepatus*). The compact body is 3D-printed in two halves, weighs 160 g, and measures 122 mm in the longest dimension without the caudal fin, which we define as one body length (BL).

A replaceable caudal fin, enabled by a magnetic connection between fin and body, allowed us to exchange fins swiftly and test a variety of fin designs in free swimming experiments. All fins were laser-cut from plastic shim material of various thicknesses and flexibilities (Artus Corp). The tail design of Finbot includes a single joint by which the passive and flexible caudal fin is connected to the main body, therefore most closely reflecting thunniform swimming [48]. Tuna-like swimmers are specialized for high-speed swimming, and feature a relatively rigid central body region for the muscular power plant that also provides inertia to avoid large recoil motions [49]. The caudal peduncle of Finbot is less tapered than peduncles of thunniform swimmers due to mechanical constraints. The caudal fin is free to rotate between symmetric and mechanically constrained limits about the neutral axis, and a sinusoidal pitching motion is prescribed by modulation

of the input power to the fin. The tail beat amplitude was held constant across all actuation frequencies and tuned to approximately 20% of the body length (figure 1(c)) since this ratio was found to minimize the energy expenditure of cruise swimming among diverse species of fish [44]; the attachment of actuators with different amplitudes is, however, possible.

We designed Finbot to be easy to replicate and modify, using off-the-shelf electronics and 3D-printed materials. Design details are shown in movie S1 and section 1 of the supplement, and an earlier version of the fin actuator is described in our previous publication [30].

3.2. Finbot's swimming performance is fish-like

Following natural scaling laws (see Methods), many fish exhibit approximately linear relationships between swimming speed and tail beat frequency [8, 9], and also a U-shaped curve for CoT with minimal values at intermediate speeds [10–12]. In mimicking fish-like swimming, Finbot showed these characteristics as well (figure 2). Finbot's cruise speed ranged from 36 mm s⁻¹ to 122 mm s⁻¹ (=BL s⁻¹) and scaled linearly with frequency for speeds greater than approximately 70 mm s⁻¹ [the experimentally identified boundary between laminar and turbulent flow, see figure 2(a)]. Strouhal number

followed the same concave up curve as is seen for a variety of fish [44, 45], and plateaued around 0.95 toward high speeds (figure 2(b)). Moreover, the drag coefficient, C_d , remained approximately constant at 0.06 across different speeds in the turbulent flow regime (supplemental figure S4(B)).

Analyzing the energetics of swimming showed that power ranged from 0.97 W to 3.3 W and scaled with frequency cubed (figure 2(c)), while approaching a finite value as f decreased (cf Methods). The nondimensional CoT was minimized to roughly 15 within a narrow range of near-optimal tail beat frequencies around 3 Hz (figure 2(d)). Finally, the Reynolds number of Finbot experiments spanned from 4,438 to 14,891 (figure 2(b)). This is in the range of small sized fish and at the transition between laminar and turbulent flow regime [45]. Consequently, the total drag of the Finbot's body is dominated by form drag rather than surface friction drag [11]. Drag measurements provided an estimate of the generated thrust forces at different swimming speeds (supplemental figure S4(A)). For instance, the drag force required to overcome while swimming at 1 BL s^{-1} was 8 mN.

3.3. Fins differ in swimming performance

Given initial results on fish-like swimming with a baseline fin, we investigated different caudal fins to identify shapes and stiffnesses that improve on speed and CoT while also exhibiting a reverse Kármán street wake characteristic of swimming fish. In a first test round, we analyzed twelve fins of different sizes, thicknesses, and shapes in two performance categories, namely speed and CoT (figures 3(a)–(c)). Additionally, we visualized the wake vortex structure for all fins (supplemental figure S6).

The search for a highly performing fin is a multi-objective optimization in which CoT and speed are correlated (figure 3(d)). We were interested in finding Pareto-optimal fins, i.e. fins that can only be improved in either CoT or speed, but not both. Using the CoT scaling law from equation (1), we fitted a Pareto-optimal frontier through the three fins 1, 3, and 6, which performed best in terms of speed or CoT (dashed line in figure 3(d)). This frontier is approximate and conservative for two reasons. First, the designs of these three fins are presumably close to an optimal design yet not completely optimal, therefore leaving margin for improvement. Second, the tail beat frequency of 2 Hz, which was used for all comparative tests, is not necessarily minimizing the U-shaped CoT. There might be frequencies which further optimize CoT without impairing speed. In order to be operated in Pareto-optimal fashion, i.e. with gains in CoT and speed conflicting, a fin must be run in the monotonically increasing region of its U-shaped CoT curve.

Since no single fin dominated in speed, CoT, and vortex structure at 2 Hz, we selected five different fins

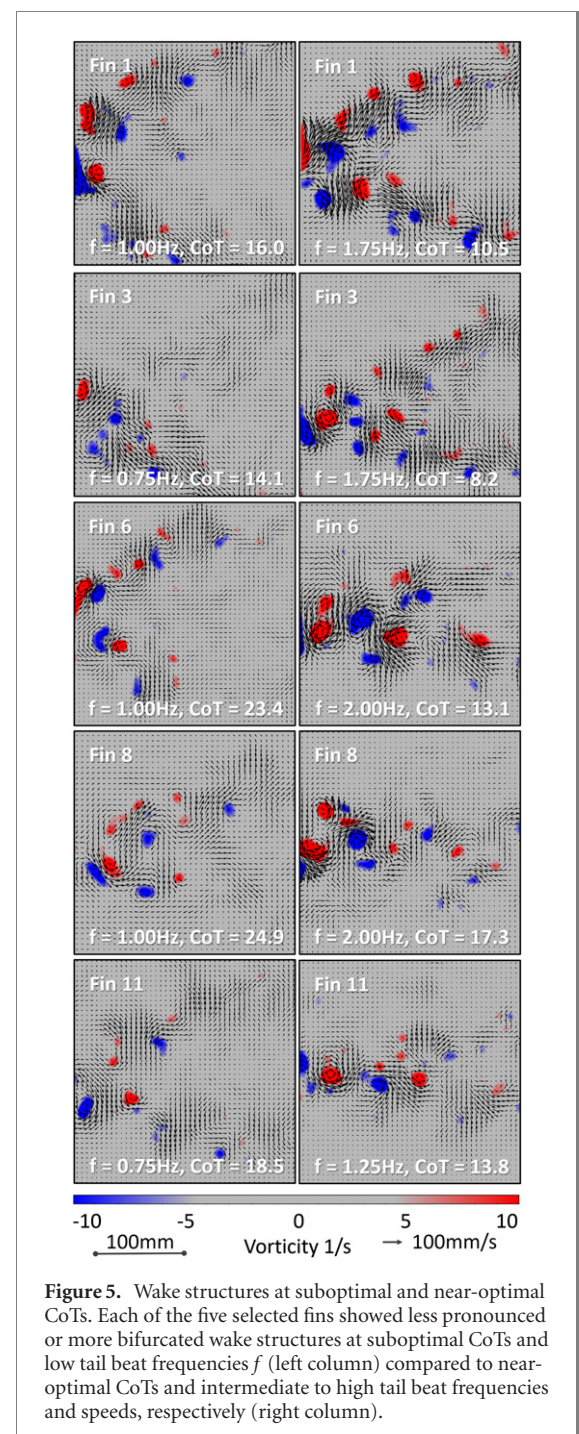
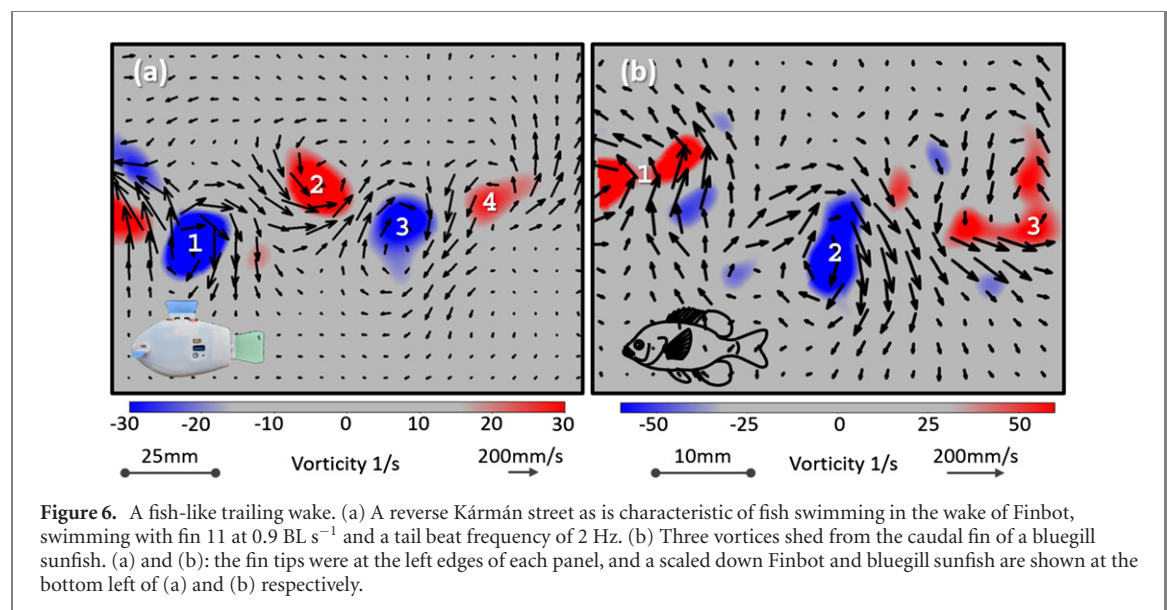


Figure 5. Wake structures at suboptimal and near-optimal CoTs. Each of the five selected fins showed less pronounced or more bifurcated wake structures at suboptimal CoTs and low tail beat frequencies f (left column) compared to near-optimal CoTs and intermediate to high tail beat frequencies and speeds, respectively (right column).

(1, 3, 6, 8, 11) for a second test round across multiple frequencies (figure 4): (i) rectangular fin 1, which co-lead in CoT with a value of 12.1 while reaching a high speed of 91.2 $mm s^{-1}$; (ii) trapezoidal fin 3 with lowest CoT of 11.1; (iii) trapezoidal fin 6 with highest speed of 115 $mm s^{-1}$; (iv) trapezoidal fin 11 with most fish-like vortex structure; and (v) tuna fin 8 to complete the mix of fin shapes [chosen over tuna fins 7 and 9 for better performance, see figures 3(b)–(d)]. The highest speed we obtained was 109 $mm s^{-1}$ ($=0.9 BL s^{-1}$) with fin 6 at 2 Hz (figure 4(a)). For operating at top speed across all frequencies, fin 11 should be chosen up to 1.25 Hz, and fin 6 from 1.5 Hz onward. The CoT analyses (figure 4(b)) confirm that



fins 1, 3, 6 perform better than fins 8 and 11. For operating at minimal CoT, fin 3 should be used at low speeds under 69 mm s^{-1} , fin 1 at intermediate speeds between 69 mm s^{-1} and 87 mm s^{-1} , and fin 6 at high speeds above 87 mm s^{-1} . The lowest CoT of 8.2 was achieved with fin 3 at a speed of 69 mm s^{-1} . The range of actuation frequencies was limited by the maximal input power and dependent on fin size and thickness and therefore varied among fins.

3.4. Minimal cost of transport and most pronounced reverse Kármán wakes are correlated

Another criterion for fin selection was fish-like vortex shedding, motivated by the goal of establishing Finbot as a platform for biomimicry. Figure 5 shows two wakes for each of the five selected fins (1, 3, 6, 8, 11)—one at low tail beat frequency and suboptimal CoT, the other one at an intermediate to high frequency and improved CoT. All fins exhibited stronger and less bifurcated wakes toward more optimal CoTs. In order to test in the region where CoT increases at the right end of the U-shaped curve, we tested fin 6 up to 4 Hz in an additional experiment (supplemental figure S7). Fin 6 exhibited its most effective and fish-like reverse Kármán wakes at minimal CoTs and intermediate speeds. Very low or high speeds led to bifurcated wake structures, which are less effective because of lateral losses.

3.5. Finbot can swim like a fish

We used bluegill sunfish (*L. macrochirus*) as model Finbot-like fish species to obtain comparative data on wake flow structure from freely-swimming fishes. Finbot and bluegill swim at similar typical speeds on the order of 1.3 BL s^{-1} and have a comparable body profile with an approximate mass and length of 138 g and 195 mm, respectively [12]. Furthermore drag forces measured on bluegill bodies are similar to those measured for the Finbot [50]. Figure 6 shows

an instance of the wake behind Finbot with fin 11 at 2 Hz and a bluegill side by side. Both exhibit a visually similar reverse Kármán street characteristic of fish swimming. These reverse Kármán streets were stable in all experiments; i.e. the wakes at other instances in time looked similar. While fin 11 yielded the most fish-like wake, several other fins including 6, 7, 8, 9, 10, were akin to fish swimming, too (see figure 5 and supplemental figures S6 and S7).

4. Discussion

The main contribution of this paper is the design and testing of an autonomous fish-like swimming robot, Finbot, with a biomimetic multi-fin configuration. Our results show that Finbot can achieve swimming behaviors characteristic of fish through selection of caudal fins that result in a reverse Kármán wake and fish-like performances regarding speed and CoT at different tail beat frequencies. Visualization of wake structures with particle image velocimetry demonstrated fish-like reverse Kármán wakes, in particular at near-optimal CoTs (figure 5). As is observed in fish, speed scaled linearly with tail beat frequency and CoT assumed a U-shaped curve when plotted against speed (figure 2). The functions we fitted to experimental data of speed, power, and CoT (figure 2) match the expected physics-based scaling relationships verified in fish biology studies [8–12, 44–47]. These functions can be used to estimate speed, power, and CoT at untested tail beat frequencies.

The search for optimal fins revealed a trade-off between speed and CoT (figure 3(d)), which illuminates why such a high variety of fins can be found amongst fish species. Fish, as opposed to our robot, have active control over the stiffness of their caudal fin [51, 52], allowing them to stiffen their fins against higher hydrodynamic loads at faster speeds [52]. The importance of fin stiffness and

its effect on propulsion were confirmed in laboratory experiments, whereby stiffer fins at higher tail beat frequencies achieve higher speeds [16, 53]. Our experiments reproduced this trend (figures 2–4). Top speed ($122 \text{ mm s}^{-1} = 1 \text{ BL s}^{-1}$) and lowest (CoT = 8.2) were achieved with two different fins (figures 2 and 4). In addition to control over fin stiffness, fish can transition between gaits to optimize their CoTs across a variety of speeds [1, 12]. Alternate fin stiffnesses and gait changes are possible for Finbot, by simply exchanging the caudal fin. This enables different objectives such as swimming at top speed with fin 6, or minimal CoT that maximizes the range of Finbot to 1,150 m with fin 3 (figure 4). Additionally, the Finbot design provides control over fin alterations beyond what we see in nature, from which a more comprehensive performance landscape can be generated.

The trade-off between speed and CoT means that there is no single best combination when pairing a robot body with a caudal fin. Beyond optimizing the shape, size, or stiffness of a fin, those parameters must be paired with suitable actuation, i.e. oscillation patterns (frequency and amplitude) that match a fin's 'assets'. When visualizing the wake structures of five different fins, we found that ideal reverse Kármán wakes predominantly occurred at minimal CoTs (figure 5). Consequently, given a robot body and a caudal fin, there are two design criteria to choose from, which both ensure effective locomotion at near-optimal CoTs: (i) running the robot at minimal CoT by measuring power and speed; (ii) confirming that vortex shedding results in a reverse Kármán street by visualizing the flow in the wake of the robot (achieved by only one piece of related work [25]).

To the best of our knowledge, Finbot is the first and smallest multi-fin autonomous underwater robot that also faithfully replicates multiple characteristics of fish swimming. Finbot is similar in speed to many small underwater robots [20, 21, 27–29]. Few other fish-based robotic designs report power consumption and CoT. The two design examples that do, the tuna-like Tunabot with a CoT of 12.7 [25] and the turtle-like Madeleine with a CoT of 0.3 [54], are difficult to compare in detail to Finbot (CoT of 8.2) since their actuation mechanism and size differ significantly. To relate Finbot's swimming performances to real fish swimming, we selected a bluegill sunfish because it is similar in body profile [12]. Finbot's maximum speed ($1 \text{ BL s}^{-1} \equiv 122 \text{ mm s}^{-1}$) is close to the typical speed of bluegill ($1.3 \text{ BL s}^{-1} \equiv 250 \text{ mm s}^{-1}$). However, comparing the CoT of Finbot ($8.2 \equiv 80.4 \text{ J kgm}^{-1}$) to bluegill ($0.25 \equiv 2.5 \text{ J kgm}^{-1}$), we note a discrepancy of an order of magnitude, hinting at an inefficient overall locomotion compared to fish. Looking at the thrust force, F , of 2.1 mN [supplemental figure S4(A)] required to overcome drag at a free swimming speed of 69 mm s^{-1} corresponding to the minimal CoT of Finbot (figure 4(b)), we can derive

the theoretical lower limit of the cost for moving a body of the shape and mass, m , of Finbot through water as $\text{CoT} = \frac{F}{m} = \frac{2.1 \text{ mN}}{160 \text{ g}} = \frac{0.013 \text{ J}}{\text{kgm}}$. This theoretical lower limit, solely imposed by Finbot's shape and mass, is below the CoT of the bluegill. Consequently, we associate Finbot's high CoT and inefficient locomotion compared to real fish with the process of generating forward speed from battery power, and assume the biggest conversion losses in the knowingly inefficient electromagnetic actuators (see supplement section 5 and [30]). In contrast, reverse Kármán wakes (figure 6) and low profile drag (supplemental figure S2) are cues for effective aquatic propulsion.

However, Finbot's propulsion could be improved by redesigning the tail region, which is currently constrained by the electromagnetic actuator (figure 1(b)). A reduced cross-sectional area of the caudal peduncle would keep the flow attached to the body and fin [supplemental figure S5(B)], and would contribute to efficient swimming [5]. Efficient undulatory fish swimming in turn manifests in constrained Strouhal numbers between 0.2 and 0.4 [4, 52]. Although the lowest Strouhal number we obtained for Finbot—0.53 with fin 6 at a tail beat frequency of 1.5 Hz and a speed of 87 mm s^{-1} , respectively—is close to the upper bound, slow speed fish locomotion often results in Strouhal numbers near 0.6 [55]. The Strouhal number of Finbot decreased with increasing swimming speeds (figure 2(b)) in a similar manner to that observed for fish locomotion [5, 55].

Fish-inspired robots are operating in the ocean already [20, 21], and our continued investigations of robotic fish swimming in the laboratory can benefit future open water designs. The ability of fish-like robotic systems to control their 3D position with multiple fins in a manner similar to freely swimming fishes will lead to more effective underwater robots that combine maneuverability and autonomous fish-like swimming. This will enable new ventures such as sampling of data in areas of high ecological sensitivity like coral reefs. The Finbot platform is also well-suited for biomimetic fish-like analyses because it achieves closed-loop fish-like swimming characteristics at a size and with maneuverability applicable to complex and repeatable laboratory experiments. With on-board measurement of power consumption, Finbot opens the door for understanding fish swimming from a new angle and can contribute to the completion of a more comprehensive view on aquatic locomotion, for example in areas like fish schooling for which we envision coordinated multi-robot experiments with camera-equipped Finbots.

Author contributions

All authors contributed to planning this research. FB and RN designed the Finbot platform. Finbot testing was conducted by FB, MS, and GVL. FB and MS

analyzed data, and FB prepared figures and an initial manuscript. All authors contributed to writing the final manuscript and gave approval for publication.

Conflict of interest

The authors declare no conflict of interests.


Acknowledgments

FB and RN were supported by the Wyss Institute for Biologically Inspired Engineering and by the Office of Naval Research (ONR Award No. N00014-20-1-2320). MS was supported by the University of South Carolina. GVL was supported by the Office of Naval Research (ONR Award No. N00014-15-1-2234).

ORCID iDs

F Berlinger  <https://orcid.org/0000-0002-9778-722X>

M Saadat  <https://orcid.org/0000-0002-3068-2538>

G V Lauder  <https://orcid.org/0000-0003-0731-286X>

R Nagpal  <https://orcid.org/0000-0001-9756-0167>

References

- [1] Lauder G V 2015 Fish locomotion: recent advances and new directions *Annu. Rev. Mar. Sci.* **7** 521–45
- [2] Sfakiotakis M, Lane D M and Davies J B C 1999 Review of fish swimming modes for aquatic locomotion *IEEE J. Ocean. Eng.* **24** 237–52
- [3] Nauen J C and Lauder G V 2002 Hydrodynamics of caudal fin locomotion by chub mackerel, *Scomber japonicus* (Scombridae) *J. Exp. Biol.* **205** 1709–24
- [4] Triantafyllou M S, Triantafyllou G S and Yue D K P 2000 Hydrodynamics of fishlike swimming *Annu. Rev. Fluid Mech.* **32** 33–53
- [5] Lighthill M J 1970 Aquatic animal propulsion of high hydromechanical efficiency *J. Fluid Mech.* **44** 265–301
- [6] Colgate J E and Lynch K M 2004 Mechanics and control of swimming: a review *IEEE J. Ocean. Eng.* **29** 660–73
- [7] von Kármán T 1963 *Aerodynamics* (New York: McGraw-Hill)
- [8] Bainbridge R 1958 The speed of swimming of fish as related to size and to the frequency and amplitude of the tail beat *J. Exp. Biol.* **35** 109–33
- [9] Rohr J J and Fish F E 2004 Strouhal numbers and optimization of swimming by *Odontoceti* cetaceans *J. Exp. Biol.* **207** 1633–42
- [10] Di Santo V, Kenaley C P and Lauder G V 2017 High postural costs and anaerobic metabolism during swimming support the hypothesis of a U-shaped metabolism-speed curve in fishes *Proc. Natl Acad. Sci. USA* **114** 13048–53
- [11] Webb P W 1975 Hydrodynamics and energetics of fish propulsion *Bull. Fish. Res. Board Can.* **190** 1–159
- [12] Kendall J L, Lucey K S, Jones E A, Wang J and Ellerby D J 2007 Mechanical and energetic factors underlying gait transitions in bluegill sunfish (*Lepomis macrochirus*) *J. Exp. Biol.* **210** 4265–71
- [13] Triantafyllou M S, Hover F S, Techet A H and Yue D K P 2005 Review of hydrodynamic scaling laws in aquatic locomotion and fishlike swimming *Appl. Mech. Rev.* **58** 226–37
- [14] Lauder G V, Lim J, Shelton R, Witt C, Anderson E and Tangorra J L 2011 Robotic models for studying undulatory locomotion in fishes *Mar. Technol. Soc. J.* **45** 41–55
- [15] Shelton R M, Thornycroft P J M and Lauder G V 2014 Undulatory locomotion of flexible foils as biomimetic models for understanding fish propulsion *J. Exp. Biol.* **217** 2110–20
- [16] Esposito C J, Tangorra J L, Flammang B E and Lauder G V 2012 A robotic fish caudal fin: effects of stiffness and motor program on locomotor performance *J. Exp. Biol.* **215** 56–67
- [17] Leftwich M C, Tytell E D, Cohen A H and Smits A J 2012 Wake structures behind a swimming robotic lamprey with a passively flexible tail *J. Exp. Biol.* **215** 416–25
- [18] Tangorra J, Phelan C, Esposito C and Lauder G 2011 Use of biorobotic models of highly deformable fins for studying the mechanics and control of fin forces in fishes *Integrative Comparative Biol.* **51** 176–89
- [19] Lauder G V, Flammang B and Alben S 2012 Passive robotic models of propulsion by the bodies and caudal fins of fish *Integrative Comparative Biol.* **52** 576–87
- [20] Katzschnmann R K, DelPreto J, MacCurdy R and Rus D 2018 Exploration of underwater life with an acoustically controlled soft robotic fish *Sci. Robot.* **3** eaar3449
- [21] Rufo M and Smithers M 2011 GhostSwimmer™ AUV: applying biomimetics to underwater robotics for achievement of tactical relevance *Mar. Technol. Soc. J.* **45** 24–30
- [22] Gibouin F, Raufaste C, Bouret Y and Argentina M 2018 Study of the thrust-drag balance with a swimming robotic fish *Phys. Fluids* **30** 091901
- [23] Long J H, Koob T J, Irving K, Combie K, Engel V, Livingston N, Lammert A and Schumacher J 2006 Biomimetic evolutionary analysis: testing the adaptive value of vertebrate tail stiffness in autonomous swimming robots *J. Exp. Biol.* **209** 4732–46
- [24] Kruusmaa M et al 2014 Filose for Svenning: a flow sensing bioinspired robot *IEEE Robot. Autom. Mag.* **21** 51–62
- [25] Zhu J, White C, Wainwright D, Di Santo V, Lauder G and Bart-Smith H 2019 Tuna robotics: A high-frequency experimental platform exploring the performance space of swimming fishes *Sci. Robot.* **4** eaax4615
- [26] Soltan K, O'Brien J, Dusek J, Berlinger F and Nagpal R 2018 Biomimetic actuation method for a miniature, low-cost multi-jointed robotic fish *OCEANS 2018 MTS/IEEE Charleston (IEEE)* pp 1–9
- [27] Tan X et al 2006 An autonomous robotic fish for mobile sensing 2006 *IEEE/RSJ Int. Conf. on Intelligent Robots and Systems (IEEE)* pp 5424–9
- [28] Berlinger F, Duduta M, Gloria H, Clarke D, Nagpal R and Wood R 2018 A modular dielectric elastomer actuator to drive miniature autonomous underwater vehicles *IEEE Int. Conf. on Robotics and Automation (ICRA 2018)* (IEEE) pp 3429–35
- [29] Aureli M, Kopman V and Porfiri M 2009 Free-locomotion of underwater vehicles actuated by ionic polymer metal composites *IEEE/ASME Trans. Mechatronics* **15** 603–14
- [30] Berlinger F, Dusek J, Gauci M and Nagpal R 2017 Robust maneuverability of a miniature, low-cost underwater robot using multiple fin actuation *IEEE Robot. Autom. Lett.* **3** 140–7
- [31] Zhong Y, Li Z and Du R 2017 A novel robot fish with wire-driven active body and compliant tail *IEEE/ASME Trans. Mechatronics* **22** 1633–43
- [32] Wen L, Liang J, Wu G and Li J 2010 Hydrodynamic experimental investigation on efficient swimming of robotic fish using self-propelled method *The Twentieth International Offshore and Polar Engineering Conf.* (International Society of Offshore and Polar Engineers)

- [33] Claphan R J and Hu H 2014 iSplash-II: realizing fast carangiform swimming to outperform a real fish *Proc. of the IEEE/RSJ Int. Conf. on Intelligent Robots and Systems (IROS 2014)* vol 1080
- [34] Xie F, Li Z, Ding Y, Zhong Y and Du R 2019 An experimental study on the fish body flapping patterns by using a biomimetic robot fish *IEEE Robot. Autom. Lett.* **5** 64–71
- [35] Wang M, Yu J and Tan M 2014 CPG-based sensory feedback control for bio-inspired multimodal swimming *Int. J. Adv. Rob. Syst.* **11** 170
- [36] Wu Z, Yu J, Su Z, Tan M and Li Z 2015 Towards an Esox lucius inspired multimodal robotic fish *Sci. China Inf. Sci.* **58** 1–13
- [37] Xie F, Zhong Y, Du R and Li Z 2019 Central pattern generator (CPG) control of a biomimetic robot fish for multimodal swimming *J. Bionic Eng.* **16** 222–34
- [38] Bal C, Ozmen Koca G, Korkmaz D, Akpolat Z H and Ay M 2019 CPG-based autonomous swimming control for multi-tasks of a biomimetic robotic fish *Ocean Eng.* **189** 106334
- [39] Yu J, Chen S, Wu Z, Chen X and Wang M 2018 Energy analysis of a CPG-controlled miniature robotic fish *J Bionic Eng.* **15** 260–9
- [40] Salazar R, Fuentes V and Abdelkefi A 2018 Classification of biological and bioinspired aquatic systems: a review *Ocean Eng.* **148** 75–114
- [41] Yu J, Wang M, Dong H, Zhang Y and Wu Z 2018 Motion control and motion coordination of bionic robotic fish: a review *J Bionic Eng.* **15** 579–98
- [42] Li S, Batra R, Brown D, Chang H-D, Ranganathan N, Hoberman C, Rus D and Lipson H 2019 Particle robotics based on statistical mechanics of loosely coupled components *Nature* **567** 361
- [43] Mathis A, Mamidanna P, Cury K M, Abe T, Murthy V N, Mathis M W and Bethge M 2018 DeepLabCut: markerless pose estimation of user-defined body parts with deep learning *Nat. Neurosci.* **21** 1281–9
- [44] Saadat M, Fish F E, Domel A, Di Santo V, Lauder G and Haj-Hariri H 2017 On the rules for aquatic locomotion *Phys. Rev. Fluids* **2** 083102
- [45] Gazzola M, Argentina M and Mahadevan L 2014 Scaling macroscopic aquatic locomotion *Nat. Phys.* **10** 758
- [46] Floryan D, van Buren T, Rowley C W and Smits A J 2017 Scaling the propulsive performance of heaving and pitching foils *J. Fluid Mech.* **822** 386–97
- [47] Floryan D, van Buren T and Smits A J 2018 Efficient cruising for swimming and flying animals is dictated by fluid drag *Proc. Natl Acad. Sci. USA* **115** 8116–8
- [48] Lindsey C C 1978 *1 - Form, function, and locomotory habits in fish* (New York: Academic Press)
- [49] Eloy C 2013 On the best design for undulatory swimming *J. Fluid Mech.* **717** 48–89
- [50] Drucker E G and Lauder G V 1999 Locomotor forces on a swimming fish: three-dimensional vortex wake dynamics quantified using digital particle image velocimetry *J. Exp. Biol.* **202** 2393–412
- [51] Alben S, Madden P G and Lauder G V 2006 The mechanics of active fin-shape control in ray-finned fishes *J. R. Soc. Interface* **4** 243–56
- [52] Flammang B E and Lauder G V 2008 Speed-dependent intrinsic caudal fin muscle recruitment during steady swimming in bluegill sunfish, *Lepomis macrochirus* *J. Exp. Biol.* **211** 587–98
- [53] Prempraneerach P, Hover F and Triantafyllou M S 2003 The effect of chordwise flexibility on the thrust and efficiency of a flapping foil *Proc. Unmanned, Untethered Submersible Technology*
- [54] Long J H Jr, Schumacher J, Livingston N and Kemp M 2006 Four flippers or two? Tetrapodal swimming with an aquatic robot *Bioinspiration Biomimetics* **1** 20
- [55] Shadwick R E and Lauder G V 2006 *Fish physiology (fish biomechanics)* (Amsterdam: Elsevier)